Journal of Applied Polymer Science

Studies on the effect of silicon carbide nanoparticles on the thermal, mechanical, and biodegradation properties of poly(caprolactone)

Thembinkosi S. Mdletshe,[1] Shivani B. Mishra,[1] Ajay K. Mishra[2]

[1]Department of Applied Chemistry, University of Johannesburg, Doornfontein, 2028 Johannesburg, South Africa

[2]Nanotechnology and Water Sustainability Research Unit, College of Engineering, Science and Technology, University of South Africa, Florida Science Campus, Johannesburg, South Africa

Correspondence to: S. B. Mishra (E-mail: smishra@uj.ac.za or bshivani73@gmail.com)

ABSTRACT: In this work, silicon carbide (SiC) nanoparticles were used to reinforce polycaprolactone (PCL). The nanocomposites were prepared by melt-mixing followed by mould extrusion. The effect of increased SiC loading on the thermal, mechanical, and dynamic mechanical properties was investigated using differential scanning calorimetry, tensile testing, and dynamic mechanical analysis (DMA), respectively. The morphology and chemical interactions were carried out by scanning electron microscopy and Fourier transform infrared spectroscopy (FTIR), respectively. The SiC nanoparticles were fairly well dispersed in the PCL matrix. FTIR indicated that there was no chemical interaction between PCL and SiC. The presence of SiC nanoparticles influenced the crystallization behavior of PCL, whereas there was no significant influence on thermal degradation behavior of PCL. Generally, the mechanical properties of the nanocomposite increased with an increase in nanoparticle content. The DMA results showed that the presence of SiC improved the storage modulus of PCL especially at higher SiC loading. Thermogravimetric analysis showed a very small influence of SiC on the thermal stability of PCL. Moreover, the glass transition temperature (T_g) of the nanocomposites shifted to lower temperatures compared to that of neat PCL. The crystal structure was not significantly influenced by the presence of SiC. The biodegradation process of PCL in soil environment delayed in the presence of SiC. © 2015 Wiley Periodicals, Inc. J. Appl. Polym. Sci. **2015**, *132*, 42145.

KEYWORDS: biodegradable; composites; crystallization; degradation; properties and characterization

Received 1 December 2014; accepted 25 February 2015

DOI: 10.1002/app.42145

INTRODUCTION

In 2010, world statistics stated that more than 10% of waste is plastic products.[1] This plastic pollution can affect different areas in the environment such as oceans, land, dams, and rivers. Plastic products are highly used compared to other materials because they can be manufactured easily, they are sold at lower prices, and they can last a long period of time in the environment because of nonbiodegradability property. An increase in population increases a demand of plastic-based products for different applications, and therefore plastic pollution increases gradually every year.[2] Plastic pollution can be reduced by three approaches, i.e., the storage of plastic waste at the dumping sites, burning of plastic waste, and recycling. However, the dumping sites are getting full gradually because of the increasing number of plastic waste. The burning process of plastics produces a large amount of carbon dioxide gas which causes the climate to change, like global warming. The burning process also produces other toxic greenhouse gases such as nitrogen dioxide, nitrogen oxide, and carbon monoxide which results in atmospheric pollution. Therefore, the plastic pollution problem is currently and safely solved by the recycling process, but this requires a large amount of labor and energy to collect the plastic waste from the environment to the recycling sites, which results in high costs and time consuming. The steps that are followed during a recycling procedure (i.e., washing, drying, separation of the waste according to the type of plastic, grinding, and reprocessing to the final product) are time consuming as well. Therefore, the whole recycling process is expensive, and the quality of the recycled plastic product is lower than the quality of a freshly synthesized product.[3]

Ninety percent of plastic products that we use every day are made by petrochemically derived polymers such as polypropylene (PP), polyethylene (PE), polystyrene (PS), polyvinyl chloride (PVC), polyethylene terephthalate (PET), and so on. These polymers are nonbiodegradable, and that is why they survive in the environment for a long time, causing a large amount of waste. Therefore, packaging industries are trying to replace these nonbiodegradable petrochemical polymers with biodegradable polymers (such as PCL, PLA, etc.) that can be biodegraded in the natural environment when they are

disposed after usage, and that can reduce plastic environmental pollution.[4,5]

A potential in biodegradable polymers as the solution for these problems has been increasing since the previous decade. There are many different types of biodegradable polymers that have been developed and studied as promising biodegradable packaging materials due to their special structure, composition, and uniquely attractive biodegradation properties.[4–6] This includes polymers such as poly(caprolactone) (PCL), poly(3-hydroxybutyrate-co-4-hydroxybutyrate) [P(3HB,4HB)], poly(lactic acid) (PLA), poly(butylene succinate) (PBS), and so on.[6] PCL is one of the most interesting biodegradable polymers for both packaging and medical applications because of its unique properties and its flexibility at room temperature. In general, PCL is a biodegradable thermoplastic polymer produced on the basis of petroleum; it consists of a sequence of methylene units between which ester groups are formed, and it is generally derived from the chemical synthesis of crude oil or by ring-opening polymerization of caprolactone using some specific catalysts. Although PCL is a promising biodegradable polymer, there are some drawbacks that have to be overcome in order to allow wide commercial applications of PCL and other biodegradable polymers. For example, PCL exhibits properties that are not suitable for other commercial uses; this includes low mechanical strength and low thermal stability which is due to its very low melting temperature (ca 65°C).[7] Nevertheless there are many different previous studies that have shown that the improvement of the properties of these biodegradable polymers by adding different nanomaterials and blending with other polymers has the great potential in designing materials that can be suitable for different commercial applications such as packaging.[1,3–10] The advantage of using nanomaterials as fillers over bulk materials is that nanofillers can improve the properties of a polymer significantly by adding a very small amount of it (e.g., 5 wt %), whereas a bulk material can improve the properties of a polymer by adding a large amount of it (e.g., 40–50 wt %), and this is because of the high surface per volume ratio of the nanomaterials.

Silicon carbide (SiC) is one of the hardest materials and it exhibits high thermal stability with a very high melting point (ca 2700°C).[11] SiC can occur in more than 250 crystalline forms called polytypes and has drawn much attraction these days as it has a good match of chemical, mechanical, and thermal properties, that makes it a semiconductor of choice for harsh environment applications including high radiation exposure, operation in high temperature, and corrosive media.[12] Therefore, because of its hardness (superior mechanical properties), nonoxide ceramic property, high thermal properties, high strength, high erosion resistance, and its resistance to chemicals, different studies have been done to strengthen and improve thermal properties of other materials (such as polymers) for industrial applications using SiC nanoparticles.[12–16] For example, Liao *et al.* prepared mHDPE/SiC nanocomposites filled with 2–8 wt % SiC via injection molding method. The results showed an increase in thermal stability and mechanical strength in the presence of SiC.[16]

Even though there are numerous studies which have been performed on incorporating various nanomaterials with PCL, there are only a few studies that have been done based on incorporating SiC with PCL. Therefore this inspired the present research to prepare PCL/SiC nanocomposites and study their properties. The main purpose of this article was to incorporate SiC nanoparticles (3C-SiC, β-SiC polytype) with PCL via melt extrusion method and study the influence of SiC nanoparticles on the thermal, mechanical, and biodegradation properties of PCL/SiC nanocomposites.

EXPERIMENTAL

Materials

PCL was supplied in pellet form by Sigma-Aldrich (Kempton Park, South Africa). It has a density of 1.145 g/mL at 25°C, polydispersity of <2, melting point of 60°C, and molecular weight (M_n) of 80,000 g/mol.

SiC (3C-SiC, β-SiC polytype) nanopowder with a particle size of <100 nm was also supplied by Sigma-Aldrich (Kempton Park, South Africa). It has a surface area of 70–90 m^2/g, melting temperature of 2700°C, and density of 3.22 g/mL at 25°C.

Sample Preparation

PCL/SiC nanocomposites with 2, 3, 4, and 5 wt % of SiC nanoparticles were prepared *via* melt mixing in a twin screw Thermo Scientific Haake Rheomixer OS instrument at 100°C, with a screw speed of 50 rpm for 10 min. The nanocomposites were prepared by melting PCL for 2 min followed by addition of SiC nanoparticles. The prepared samples were then melt-extruded at a temperature range of 100–120°C using a single screw extruder with a screw speed of 50 rpm to form a sheet of 50 × 0.5 mm.

Characterization Techniques

Fourier Transform Infrared Spectroscopy (FTIR). FTIR spectra of neat PCL, SiC nanopowder, and the nanocomposites were obtained using Perkin Elmer Spectrum 100 FTIR spectrometer at room temperature. The spectra of thin films were recorded using four scans over the range of 4000–650 cm^{-1}.

Scanning Electron Microscopy (SEM). The morphology or the distribution of SiC nanoparticles in the PCL matrix was studied using a VEGA3 Tescan Scanning Electron Microscopy. All samples were frozen in liquid nitrogen for 15 min and fractured while they were still inside the liquid nitrogen. The fractured samples were then sputter-coated with gold for 60 s to improve the conductivity and allowed to dry. The fracture surfaces were then viewed using an accelerating voltage of 5 kV.

Differential Scanning Calorimetry (DSC). The influence of the SiC nanoparticles on the melting behavior of the PCL polymer matrix was studied by DSC. The analyses were performed by Perkin Elmer Differential Scanning Calorimeter Pyris 1. Samples with masses between 5 and 10 mg were sealed in aluminum pans and heated under nitrogen flow of 20 mL/min from −35 to 90°C at a heating rate of 10°C/min, held at this temperature for 1 min to erase the thermal history, cooled to −35°C at the same rate, and reheated to 90°C under the same conditions. The melt crystallization temperature (T_c) and the crystallization enthalpy (ΔH_c) were obtained from the cooling curves, whereas the melting temperature (T_m) and the melting enthalpy (ΔH_c) were obtained from the second heating curves.

Thermogravimetric Analysis (TGA). Thermogravimetric analyses were carried out to study the thermal stabilities of the nanocomposite samples using a Perkin Elmer STA 6000 Simultaneous Thermal Analyzer. Samples with masses which ranged from 20 to 25 mg were heated under nitrogen atmosphere (20 mL/min) from ambient temperature to 600°C at a heating rate of 10°C/min, and corresponding mass loss was recorded.

Dynamic Mechanical Analysis (DMA). For thermomechanical properties, a storage modulus and tan δ of the samples were determined in a Perkin Elmer Diamond Dynamic Mechanical Analyzer (DMA). Rectangular bar specimens with dimensions of a length of 50 mm, width ranged from 10.08 to 10.20 mm, and thickness ranged from 0.57 to 0.74 mm were used for this study. The measurements were carried out in the dual cantilever tension mode and corresponding viscoelastic properties were determined as a function of temperature. The samples were heated under nitrogen from −90 to 40°C at a scanning rate of 3°C/min, and at a frequency of 1 Hz.

Mechanical Property Test. The mechanical properties of the neat PCL and the nanocomposites were determined using a Tinius Oisen Horizon H5KS Hounsfield Tensile tester instrument at a speed of 10 mm/min at ambient temperature. The rectangle-shaped samples with a width ranged from 12.90 to 13.10 mm and the thickness ranged from 0.66 to 0.78 mm were used. The stress and the elongation at break, Young's modulus, as well as tensile strength were determined from stress–strain curves. At least five samples were tested for each composition, and the average values were reported.

Wide Angle X-ray Diffraction (XRD). The effect of SiC nanoparticles on the crystal structure and morphology of the PCL/SiC nanocomposites was studied by WAXD technique. This was achieved by using a Phillips Powder X'Pert^3 X-ray Diffractometer with Cu Kα1 radiations. The sample films were placed and mounted onto the glass sample holders. All measurements were done at a range of $2\theta = 4$–$90°$ using a step size of $2\theta = 0.02°$ at room temperature using XPERT-PRO wide angle diffractometer system. The following operating conditions were used: current (I) of 40 mA and a voltage (V) of 40 kV.

Biodegradation Studies. The influence of SiC nanoparticles on the biodegradation process of PCL was achieved by the indoor soil burial test method.[17] The CULTERRA professional potting soil used was formulated from 100% organic raw materials derived from COCO peat, forest products, and water retentive agents. Basically, a PVC plastic flower pot was used as the soil container.[18] Three rectangular shaped samples (0.5–0.7 mm thick) per nanocomposite were horizontally buried at 5–7 cm depth to ensure aerobic degradation conditions. The PVC container (with buried samples) was left in an incubator and the soil temperature set to range from 35–40°C. The soil was watered regularly (everyday) to keep it moist and to prevent anaerobic biodegradation. The samples were taken out of the soil after every 1 week, thoroughly washed with distilled water, and dried at room temperature to constant weight. Photographs of the samples taken before and after the test were compared and used to understand the influence of SiC on the biodegradation process of PCL.

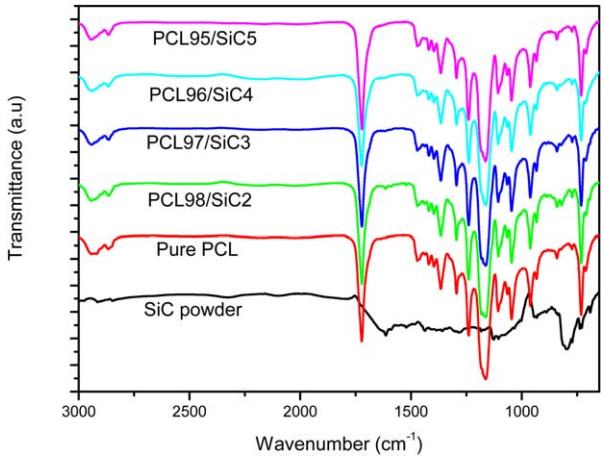

Figure 1. FTIR spectra of pure PCL and PCL/PCL nanocomposites with different SiC content. [Color figure can be viewed in the online issue, which is available at wileyonlinelibrary.com.]

RESULTS AND DISCUSSION

Fourier Transform Infrared Spectroscopy

FTIR spectra of SiC powder as received, pure PCL, and PCL/SiC nanocomposites with different SiC contents are shown in Figure 1. A strong broader absorption peak at 799 cm^{-1} for SiC powder was observed, and it is related to the stretching vibration of the Si—C bond of the crystalline β-SiC phase.[12,14,19,20]. The spectrum of pure PCL shows a strong sharp absorption peak at 1718 cm^{-1} related to the stretching vibrations of C═O bonds, a broad absorption peak at 3000–2800 cm^{-1} related to the stretching vibrations of CH_2, a strong broader absorption peak at 1165 cm^{-1} related to the aliphatic ether stretching vibrations of C—O—C bonds, a sharp absorption peak at 731 cm^{-1} related to the long-chain rocking motion vibrations of —CH_2, a sharp absorption at 1468 cm^{-1} related to the bending vibrations of —CH_2, and a peak at 1362 cm^{-1} related to the bending vibrations of —CH.[21] By comparing the spectra of the PCL/SiC nanocomposites with one of the pure PCL, it can be seen that the nanocomposites displayed similar characteristic peaks of pure PCL. This means that there was no strong chemical interaction between PCL and SiC nanoparticles, only a physical interaction took place between PCL matrix and SiC nanoparticle, and this may be due to the small amount of SiC added (i.e., 2–5 wt %). This phenomenon was also reported by Then *et al.* who added Tapioca Starch Blends by Octadecylamine modified clay in PCL.[22]

Scanning Electron Microscopy

SEM images of the fractured surfaces of (a) pure PCL, and PCL/SiC nanocomposites with (b) 2, (c) 3, (d) 4, and (e) 5 wt % of SiC nanoparticles are shown in Figure 2. It can be clearly seen that pure PCL [Figure 2(a)] is a smooth surface without any white spots. In the case of PCL/SiC nanocomposites [Figure 2(a–e)], small white spots are observed and can be related to the SiC nanoparticles dispersed in the PCL matrix. It can be seen that these spots increase with an increase in the wt % of

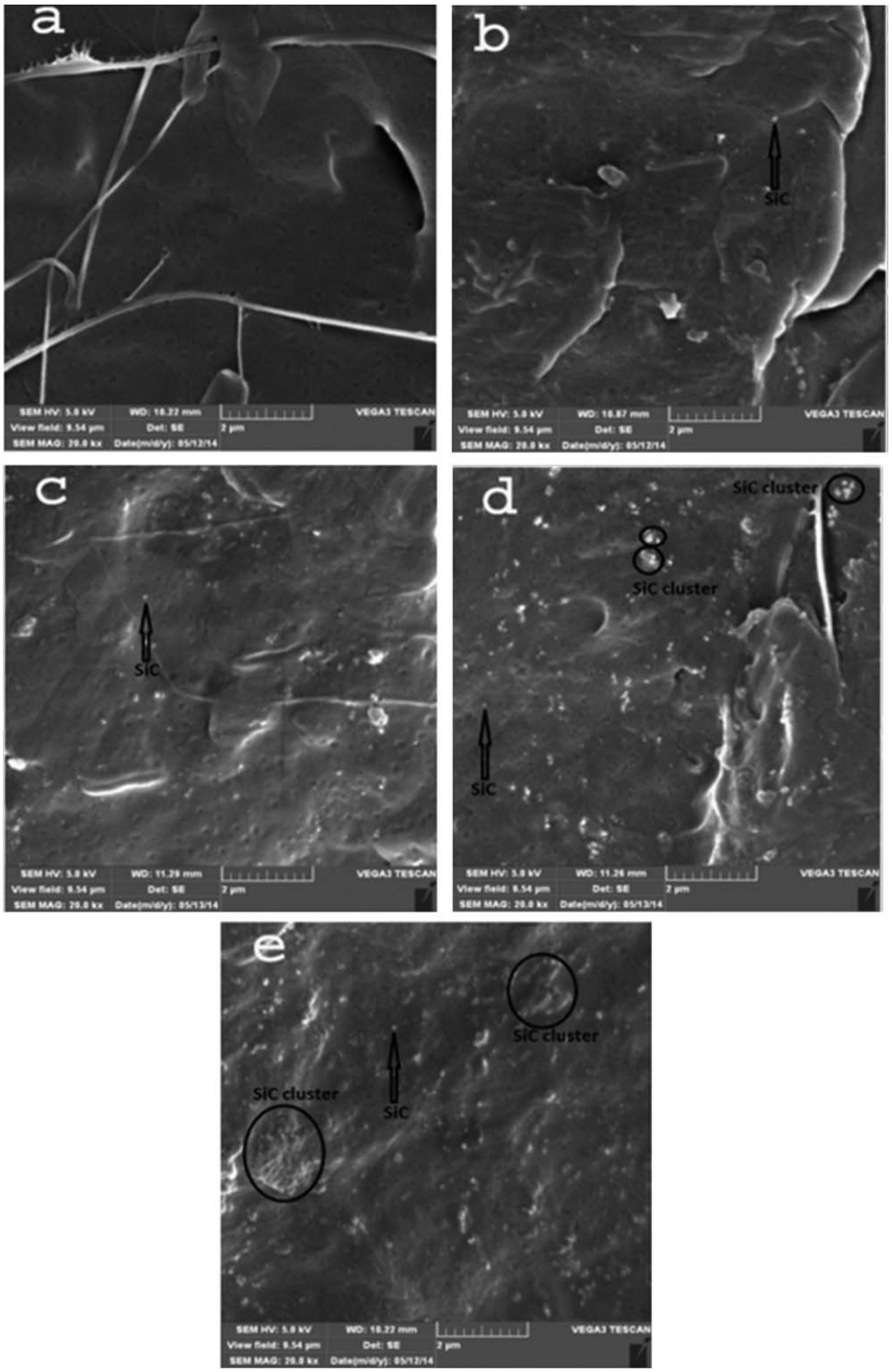

Figure 2. SEM images of (a) pure PCL, (b) PCL98/SiC2, (c) PCL97/SiC3, (d) PCL96/SiC4, and (e) PCL95/SiC5.

SiC nanoparticles [Figure 2(b–e)]. At low content of SiC in the nanocomposite materials, the nanoparticles were fairly dispersed [Figure 2(b,c)]. Interestingly, the size of these nanoparticles was smaller in these compositions with an average diameter of about 49.1 nm. The PCL/SiC nanocomposite with 4 wt % of SiC [Figure 2(d)] also shows a good distribution of SiC, but a few small SiC clusters of about 0.3 μm in diameter started to develop. Figure 2(e) (with 5 wt % SiC) shows the clear agglomerated SiC nanoparticles that formed some big SiC clusters of about 1.5 μm in diameter. However, some SiC nanoparticles in Figure 2(e) are still well dispersed in the PCL matrix as in Figure 2(b–d). Therefore, the SEM results in Figure 2 show that the SiC nanoparticles are well dispersed in the PCL matrix at lower content, but start to agglomerate as the content increases from

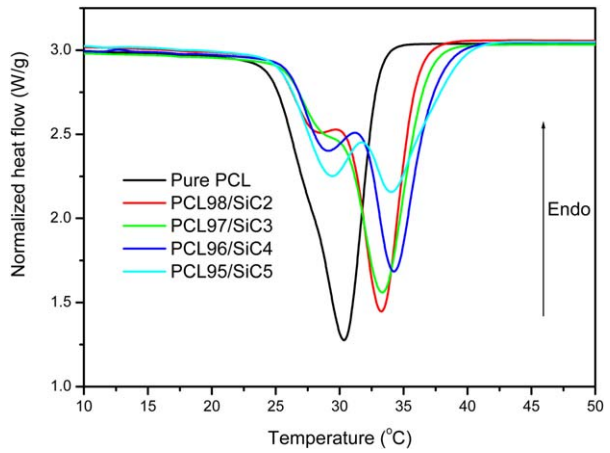

Figure 3. DSC cooling exotherms of a pure PCL and its PCL/SiC nanocomposites with different SiC content. [Color figure can be viewed in the online issue, which is available at wileyonlinelibrary.com.]

4 to 5 wt %. This is a common phenomenon, and it has been reported by different authors that the inorganic nanoparticles tend to agglomerate as the wt % content increases in the polymer matrix due to the large surface areas. This is supported by the SEM results obtained by Liao *et al.* who observed the agglomeration of SiC nanoparticles in a polyamide6 matrix at a higher content of 5 wt % and above.[23]

Differential Scanning Calorimetry

DSC thermograms of the cooling curves showing the crystallization behavior of pure PCL and its PCL/SiC nanocomposites are shown in Figure 3. The exothermic peaks in Figure 3 represent the melt crystallization temperatures (T_c) of the samples. The crystallization temperatures and crystallization enthalpies (ΔH_c) obtained in Figure 3 are tabulated in Table I. It can be seen from Figure 3 and Table I that the T_c increased from 30.35 to 34.30°C as the SiC content increased up to 4 wt %, but slightly decreased to 34.07°C for 5 wt % SiC content. The decrease of T_c for 5 wt % SiC composite is due to the agglomeration supported by the SEM results in Figure 2.[23] This means that SiC nanoparticles promoted the crystallization process of PCL by acting as the nucleating agents for the crystallization, and this is known as heterogeneous nucleation. An increase in T_c is directly proportional to an increase in lamellar thickness of the crystallites formed. The promotion of the PCL crystallization process by SiC nanoparticles is also supported by the increase of the crystallization onset temperature as the amount of SiC increases, as shown in Figure 3. The second crystallization peak developed in the presence of SiC and its size increased as the amount of SiC increased. For each composite, it is believed that the first peak at higher temperatures is due to crystallites that were formed heterogeneously (with the presence of SiC nanoparticles as nucleating agents) and the second peak at lower temperatures is due to the crystallites that were formed homogeneously (without SiC as the nucleating agent).

The degree of crystallinity (χ_c) of the prepared pure PCL and its PCL/SiC nanocomposites was calculated using the following equation:

$$\chi = \frac{\Delta H_m}{\Delta H_m^0 \times \left(1 - \frac{\text{wt } \%_{SiC}}{100}\right)} \times 100\% \quad (1)$$

where ΔH_m is the specific melting enthalpy of the tested sample, ΔH_m^0 is the specific melting enthalpy of the 100% crystalline PCL, i.e., 142.0 J/g,[24] and wt $\%_{SiC}$ is the weight percentage of the SiC nanoparticle present in that particular composite. The calculated crystallinity values were then tabulated in Table I. From Table I, it can be seen that the presence of SiC nanoparticles increased the degree of crystallinity of PCL from 31.61 to 35.20%, and this was due to the promotion of the PCL crystallization process caused by the presence of SiC which acted as the nucleating agent. The composite of 4 wt % SiC content showed the highest crystallinity of 35.20%, whereas the crystallinity decreased to 33.75% as the SiC content increases to 5 wt % and this was due to the agglomeration of SiC nanoparticles supported by the SEM results in Figure 2.

DSC thermograms of the second heating curves showing the melting behavior of pure PCL and its PCL/SiC nanocomposites are shown in Figure 4. The endothermic peaks in Figure 4 represent the melting temperatures of the crystallites formed during the cooling process in Figure 3. The melting temperatures (T_m) and melting enthalpies (ΔH_m) obtained in Figure 4 are also tabulated in Table I. It can be seen from Figure 4 and Table I that the T_m increased from 55.93 to 56.47°C as the SiC content increases up to 4 wt % but decreased to 55.93°C for the 5 wt % SiC composite, and this is due to the decrease of T_c (reduced lamellar thickness) in Figure 3 which was due to the agglomeration of SiC supported by the SEM results. This is because the lamellar thickness of the formed spherulitic crystallites is directly proportional to the T_c and T_m which is commonly proportional to the degree of crystallinity of the sample. There is a very small influence of SiC nanoparticles on the melting behavior of PCL observed as compared to the crystallization behavior and only one peak was observed for the melting of the nanocomposites. This phenomenon was also

Table I. DSC Data from Cooling and Second Heating Curves

Sample	T_c (°C)	ΔH_c (J/g)	T_m (°C)	ΔH_m (J/g)	Crystallinity χ_c (%)
Pure PCL	30.35 ± 0.01	47.89 ± 0.99	55.93 ± 0.34	44.88 ± 1.14	31.61
PCL98/SiC2	33.22 ± 1.85	50.31 ± 2.27	56.13 ± 0.23	45.39 ± 0.85	32.62
PCL97/SiC3	33.31 ± 0.17	49.87 ± 1.69	56.29 ± 0.09	44.86 ± 1.60	32.57
PCL96/SiC4	34.30 ± 0.44	48.77 ± 0.63	56.47 ± 0.48	47.99 ± 2.36	35.20
PCL95/SiC5	34.07 ± 0.09	48.72 ± 2.18	55.93 ± 0.26	45.54 ± 0.97	33.76

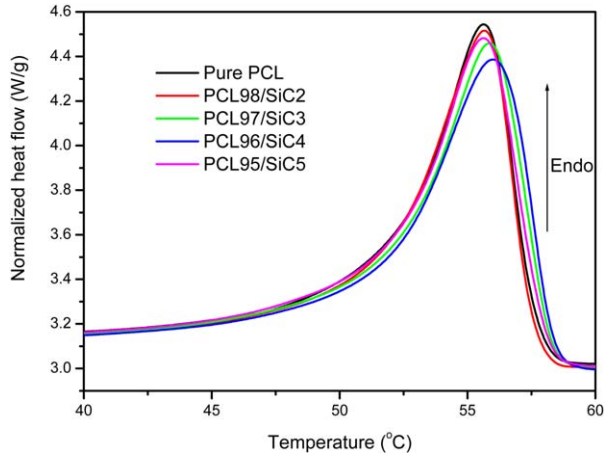

Figure 4. DSC second heating endotherms of a pure PCL and its PCL/SiC nanocomposites with different SiC content. [Color figure can be viewed in the online issue, which is available at wileyonlinelibrary.com.]

recently reported by Bonilla *et al.* who used titania nanoparticles as a filler.[25] This is because as the temperature increased, all the crystallites of the same polymer present in the sample started to be disordered (or melt) in the same manner. Since there is no chemical interaction (supported by FTIR results in Figure 1), the physical interaction between SiC and PCL decreased as the temperature is increased because the polymer chains started to move away from the SiC particles at higher temperatures and become independent.

Thermogravimetric Analysis

TGA curves representing the thermal degradation behavior of pure PCL and its PCL/SiC nanocomposites under a nitrogen atmosphere are shown in Figure 5. The thermal degradation of PCL under inert atmosphere, such as nitrogen, occurs through the rupturing of the polyester chains via the ester pyrolysis reaction with the release of carboxylic acid groups, water, and carbon dioxide gas. When two pyrolysis reactions occur with the ester functions along the chain during thermal degradation of PCL under inert atmosphere, the 5-hexenoic is most probably

Table II. TGA Data from Figure 5

Sample	$T_{50\%}$ (°C)
Pure PCL	414.34
PCL98/SiC2	414.83
PCL97/SiC3	415.00
PCL96/SiC4	415.02
PCL95/SiC5	415.89

formed.[24] The values of $T_{50\%}$ obtained from Figure 5 are tabulated in Table II. It can be seen from Figure 5 and Table II that the addition of SiC nanoparticles has no considerable influence on the thermal stability of PCL. There is a slight increase in $T_{50\%}$ value from 414.34 to 415.89°C with an addition of SiC (Table II). Nevertheless these nanocomposites displayed the formation of a char up to 600°C in the presence of SiC (Figure 5), and this char was attributed to the remainder of SiC nanoparticles. These TGA results also support the idea that there was a poor interaction between SiC and PCL at high temperatures. This is because the amount of char formed equals the amount of SiC present in that composite (e.g., 3% of char remained for a composite that contains 3 wt % of SiC), and this shows that the PCL chains and SiC nanoparticles were independent of each other at high temperatures. This phenomenon was also reported by Dash *et al.* who got no influence of SiC addition up to 10 wt % on the thermal stability of starch but only an increase in char was observed as the amount of SiC increased.[12] Similarly, Bonilla *et al.* showed no influence of titania (TiO_2) nanoparticles on the thermal stability of PCL by adding up to 5 wt % of titania.[25]

Dynamic Mechanical Analysis

Storage modulus (E') of pure PCL and its PCL/SiC nanocomposites as a function of temperature are represented in Figure 6. It can be seen from Figure 6 that the storage modulus decreases radically at a temperature around −60°C. This is due to the relaxation or mobility of PCL chains during its glass transition (T_g) which is at around −60°C.[24] It can be seen that at a glassy state (below T_g), the nanocomposites with 2, 3, and 4 wt % of SiC

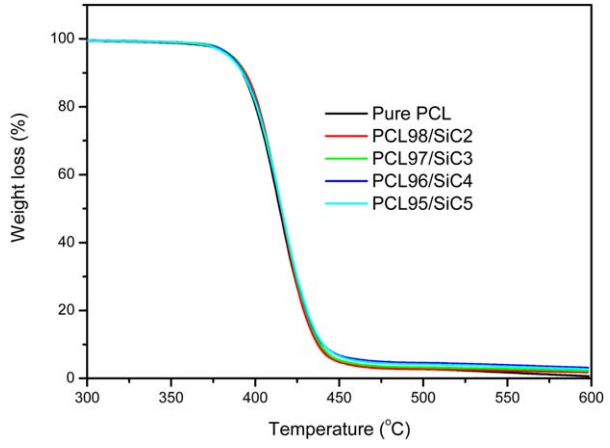

Figure 5. TGA curves of a pure PCL and its PCL/SiC nanocomposites with different SiC content. [Color figure can be viewed in the online issue, which is available at wileyonlinelibrary.com.]

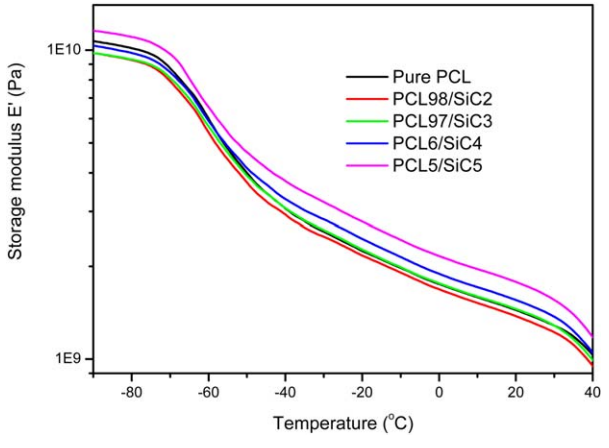

Figure 6. Storage modulus curves of a pure PCL and its PCL/SiC nanocomposites with different SiC content. [Color figure can be viewed in the online issue, which is available at wileyonlinelibrary.com.]

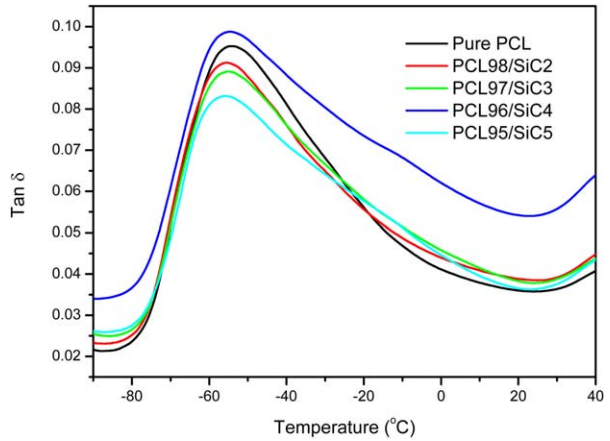

Figure 7. Tan δ curves of a pure PCL and its PCL/SiC nanocomposites with different SiC content. [Color figure can be viewed in the online issue, which is available at wileyonlinelibrary.com.]

show a lower storage modulus compared to the pure PCL. However, the nanocomposite with 5 wt % of SiC shows a higher storage modulus than pure PCL over the whole range of temperatures investigated, whereas the nanocomposite with 2 wt % of SiC shows a lower storage modulus than pure PCL over the whole range of temperatures investigated. It seems as if the SiC acted as the plasticizer at a lower content (i.e., 2 wt % of SiC).[24] Generally, the SiC enhanced the storage modulus at higher temperatures (above T_g), but the reinforcement was more pronounced at higher SiC content.

tan δ as a function of temperature also showing the thermomechanical behavior of pure PCL and its PCL/SiC nanocomposites at a temperature range of −90 to 40°C is represented in Figure 7. In this study, the T_g was taken as the maximum point of a tan δ curve. The tan δ curves in Figure 7 shows a relaxation of PCL chains at a temperature around −55°C. This relaxation is also related to the mobility of PCL chains during its glass transition (T_g).[26] Therefore the temperature at the maximum point of a tan δ curve represents the T_g of that material. These T_g values from Figure 7 are tabulated in Table III. It can be seen from Figure 7 and Table III that the peak shifted slightly toward the lower temperatures in the presence of SiC, which means that the presence of SiC smoothened the sliding of the amorphous PCL chains over the surface of the formed crystallites. In other words, this may be due to the smooth surface crystallites formed in the presence of SiC and/or due to the few entanglements formed in the amorphous regions in the presence of SiC.

Table III. DMA Data Obtained from Figure 7

Sample	T_g (°C)
Pure PCL	−53.55
PCL98/SiC2	−55.20
PCL97/SiC3	−54.76
PCL96/SiC4	−54.88
PCL95/SiC5	−56.08

Mechanical Property Test

The values obtained from the stress–strain curves were tabulated in Table IV. It can be seen from Table IV that the Young's modulus increased by 36.46% as the amount of SiC increases up to 5 wt %. This increase in Young's modulus is attributed to SiC imparting rigidity to the nanocomposite material. This can also be due to a strong physical interaction between the PCL chains and SiC at room temperature resulting from the large interfacial area between SiC particles and the matrix.[27] The tensile strength increased by 20.18% as the amount of SiC increased up to 4 wt %. This increase in tensile strength is due to the good dispersion of SiC nanoparticles in a matrix as seen in the SEM results. The increase in the crystallinity (supported by DSC) also contributed to an increase of the tensile strength because the higher the crystallinity, the stiffer the material. By adding more SiC, up to 5 wt %, the tensile strength decreased. This may be attributed to the decreased crystallinity (from DSC results) and agglomeration (supported by SEM). These agglomerates acted as the defect points where stress cracking occurred more easily. The stress at yield also increased by adding SiC up to 5 wt %, which means the ability of the polymer to fight against deformation increased in the presence of SiC (this is proportional to the Young's modulus). The toughness (strain at break) also increased as the amount of SiC increased up to 4 wt %, this is due to the decrease in T_g (supported by DMA) which was due to an increase in the flexibility of the amorphous regions. The flexibility decreased by adding 5 wt % of SiC due to the mentioned agglomeration. This phenomenon of increasing the tensile strength which decreases at higher filler content has been reported by many authors.[22,23,27] Generally, the well-dispersed SiC nanoparticles stiffened PCL by increasing the tensile strength, whereas the agglomerated SiC nanoparticles slightly decreased the tensile strength.

Wide Angle X-ray Diffraction (WAXD)

WAXD diffractograms of pure PCL and its PCL/SiC nanoparticles are represented in Figure 8. The peak positions, d-spacing

Table IV. Tensile Data Obtained from the Stress–Strain Curves

Sample	Stress at yield (MPa)	Tensile strength (MPa)	Strain at brake (%)	Young's Modulus (MPa)
Pure PCL	15.3 ± 0.3	22.3 ± 1.1	2889 ± 63	87.6 ± 3.3
PCL98/SiC2	15.4 ± 0.6	22.9 ± 1.0	2923 ± 117	94.7 ± 6.1
PCL97/SiC3	16.1 ± 0.3	25.6 ± 2.6	3022 ± 220	96.2 ± 3.8
PCL96/SiC4	17.0 ± 0.6	26.8 ± 2.1	3063 ± 150	102.8 ± 5.4
PCL95/SiC5	17.5 ± 0.5	24.9 ± 2.9	2874 ± 257	119.5 ± 2.2

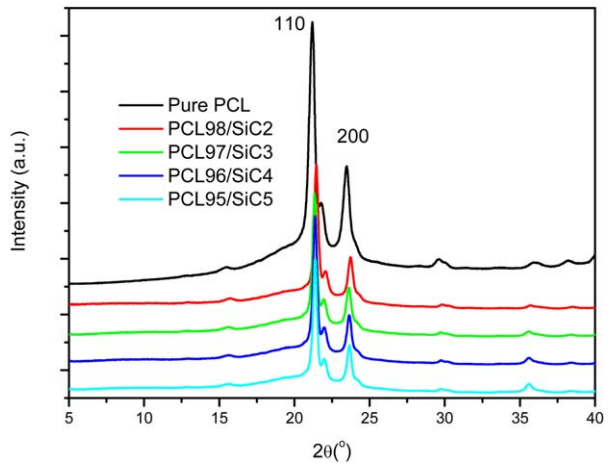

Figure 8. WAXD diffractograms of pure PCL and its PCL/SiC nanocomposites. [Color figure can be viewed in the online issue, which is available at wileyonlinelibrary.com.]

values, and the full width at half maximum (FWHM) values are tabulated in Table V. It can be clearly seen from Figure 8 that both pure PCL and the PCL/SiC nanocomposites show a broad halo peak that is overlapped by a sharp peak at 2θ of 21.2° (110) and 23.5° (200) for pure PCL. This broad halo peak is related to the amorphous fractions whereas the two sharp peaks (i.e., 110 and 200 Miller indices) are related to the orthorhombic crystal structure of PCL.[28,29] By comparing the diffractograms in Figure 8, it can be clearly seen that the size of the broad halo peak decreased in the presence of SiC and the two sharp peaks became quiet narrow in the presence of SiC. This means that the presence of SiC nanoparticles increased the degree of crystallinity of PCL. This also supports the increase in crystallinity obtained from the DSC results. The FWHM, 2θ, and d-spacing values in Table V show a slight change in the presence of SiC. Since these values are related to the crystal structure or dimension, the presence of SiC did not influence the crystal perfection significantly.

Biodegradation Studies

Figure 9 shows the images of the samples taken before and after the biodegradation test carried out in an incubator at a temperature range of 35–40°C. It can clearly be seen from Figure 9 that samples showed surface degradation with roughening and the formation of holes on the surface after 2 weeks, and that surface degradation increased as the burial time increased. The soil particles were highly adhered on the sample surfaces after

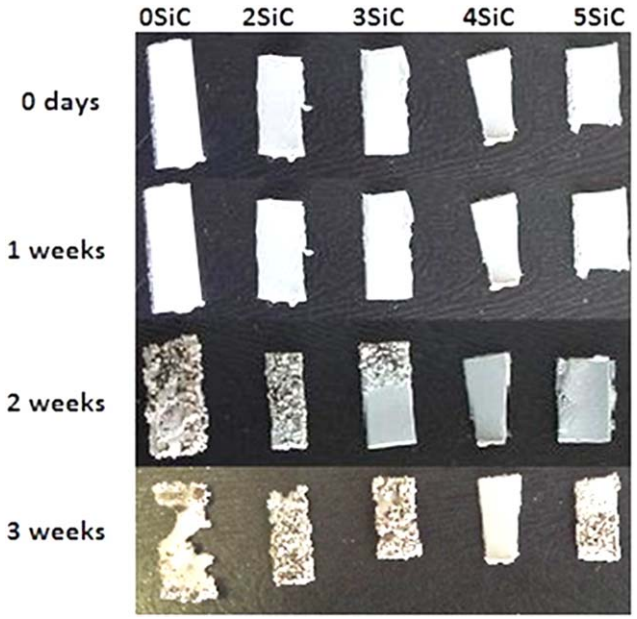

Figure 9. Photographs of pure PCL and its PCL/SiC nanocomposites before (0 days) and after 1, 2, and 3 weeks in soil. [Color figure can be viewed in the online issue, which is available at wileyonlinelibrary.com.]

degradation and that increased the weight of the samples after the biodegradation test. By comparing the photographs in Figure 9, it can be seen that the presence of SiC nanoparticles delayed the biodegradation process of PCL because pure PCL showed serious sample damage after 3 weeks, whereas the nanocomposites only showed surface roughening after 3 weeks. The PCL96/SiC4 nanocomposite did not show any surface roughening throughout the test. This is because the higher the crystallinity, the slower the biodegradation process. It is known that microorganisms attack amorphous fractions more easily than crystalline fractions.[17] Therefore, this is why PCL96/SiC4 remained stable because it is the one that showed the highest crystallinity from the DSC results. The biodegradation process started by the adhering of microorganisms (on the sample surface), followed by the growth of the microorganisms on the sample surface. Therefore, it is believed that the microorganisms used the first week to adhere and settle on sample's surfaces. The main chain scission mechanism during the biodegradation of PCL in soil proceeds via chemical and biological hydrolysis, so the biodegradation process is highly dependent on the water availability that promotes the microbial attack and the hydrolysis of the matrix.[17] It has been reported that the PCL

Table V. WAXD Data of Pure PCL and Its PCL/SiC Nanocomposites

	110			200		
Sample	2θ (°)	d-spacing (Å)	FWHM	2θ (°)	d-spacing (Å)	FWHM
Pure PCL	21.2	4.19	0.368	23.5	3.79	0.268
PCL98/SiC2	21.5	4.14	0.268	23.7	3.75	0.251
PCL97/SiC3	21.3	4.16	0.284	23.6	3.77	0.218
PCL96/SiC4	21.4	4.16	0.251	23.7	3.76	0.251
PCL95/SiC5	21.4	4.16	0.251	23.7	3.76	0.234

biodegradation process in soil generally occurs through an inhomogeneous mechanism.[30] Therefore, the more degraded areas are because of better contact between the sample surface and soil and/or because of the inhomogeneous growth of microorganisms on the sample surface.

CONCLUSION

PCL/SiC nanocomposites were successfully prepared by the melt-mixing method. The chemical bonding between PCL and SiC was not observed by FTIR indicating a physical interaction among the polymer matrix and the filler nanoparticles. A good dispersion of SiC nanoparticles in a PCL matrix especially at a lower SiC contents was observed from SEM images, whereas agglomeration was observed at higher SiC contents. The presence of SiC nanoparticles increased the crystallinity, melting temperature, and melt crystallization temperature of PCL by acting as crystallization nucleating agents. Interestingly, a decrease in the glass transition temperature of PCL in the presence of SiC nanoparticles was observed, and this is believed to be due to the reduction of entanglements in the presence of SiC nanoparticles. An increase in storage modulus in the presence of SiC was also observed, but this was more pronounced at higher contents of SiC nanoparticles. A very small influence of SiC nanoparticles on the thermal stability was observed. Young's modulus, toughness, and tensile strength of PCL increased in the presence of SiC nanoparticles. A crystal structure or crystal dimension was not significantly influenced by the presence of SiC. The presence of SiC delayed the biodegradation process of PCL in a soil environment. In conclusion, PCL was successfully reinforced with SiC nanoparticles, and the presence of SiC nanoparticle influenced the mechanical, thermomechanical, thermal, and biodegradation properties of PCL as expected. In conclusion, PCL was successfully reinforced with SiC nanoparticles, and the presence of SiC nanoparticle influenced the mechanical, thermomechanical, thermal, and biodegradation properties of PCL as expected.

ACKNOWLEDGMENTS

The authors would like to appreciate the financial support from the Department of Science and Technology (DST) under the National Nanoscience Postgraduate Teaching and Training Platform (NNPTTP), National Research Foundation, South Africa together with the University of Johannesburg.

REFERENCES

1. Fukushima, K.; Tabuani, D.; Abbate, C.; Arena, M.; Ferreri, L. *Polym. Degrad. Stab.* **2010**, *95*, 2049.
2. Fomin, V. A.; Guzeev, V. V. *Prog. Rubber Plast. Technol.* **2001**, *17*, 186.
3. Yiu-Wing, M.; Zhong-Zhen, Y. Polymer Nanocomposites; Woodhead Publishing Limited: Cambridge, **2006**.
4. Raquez, J. M.; Habibi, Y.; Murariu, M.; Dubois, P. *Prog. Polym. Sci.* **2013**, *38*, 1504.
5. Handbook of Biopolymers and Biodegradable Plastics. Synthesis, Properties, Environmental and Biomedical Applications of Polylactic Acid. Available at: http://dx.doi.org/10.1016/B978-1-4557-2834-3.00009-4 [accessed on February 28, (2014)].
6. Rhim, J. W.; Park, H. M.; Ha, C. S. *Prog. Polym. Sci.* **2013**, *38*, 1629.
7. Singh, R. P.; Pandey, J. K.; Rutot, D.; Degee, P.; Dubois, P. *Carbohydr. Res.* **2003**, *338*, 1759.
8. Wu, C. S. *Polymer* **2005**, *46*, 147.
9. Rosa, D. S.; Guedes, C. G. F.; Bardi, M. A. G. *Polym. Test.* **2007**, *26*, 209.
10. Li, X. Y.; Kong, X. Y.; Shi, S.; Wang, X. H.; Guo, G.; Luo, F.; Zhao, X.; Wei, Y. Q.; Qian, Z. Y. *Carbohydr. Polym.* **2010**, *82*, 904.
11. Guo, Z.; Kim, T. Y.; Lei, T.; Pereira, T.; Sugar, J. G.; Hahn, H. T. *Compos. Sci. Technol.* **2008**, *68*, 164.
12. Dash, S.; Swain, S. K. *Carbohydr. Polym.* **2013**, *97*, 758.
13. Han, S.; Chung, D. D. L. *Appl. Clay Sci.* **2013**, *83–84*, 375.
14. Majewski, P.; Choudhury, N. R.; Spori, D.; Wohlfahrt, E.; Wohlschloegel, M. *Mater. Sci. Eng. A* **2006**, *434*, 360.
15. Liao, C. Z.; Bao, S. P.; TJong, S. C. *Adv. Polym. Technol.* **2011**, *30*, 322.
16. Liao, C. Z.; Bao, S. P.; TJong, S. C. *Compos. Interfaces* **2011**, *18*, 107.
17. Ludueña, L.; Vázquez, A.; Alvarez, V. *Carbohydr. Polym.* **2012**, *87*, 411.
18. Bastioli, C.; Cerutti, A.; Guanella, I.; Romano, G. C.; Tosin, M. *J. Environ. Polym. Degrad.* **1995**, *3*, 81.
19. Cao, J. P.; Zhao, J.; Zhao, X.; Hu, G. H.; Dang, Z. M. *J. Appl. Polym. Sci.* **2013**, *130*, 638.
20. Mavinakuli, P.; Wei, S.; Wang, Q.; Karki, A. B.; Dhage, S.; Wang, Z.; Young, D. P.; Guo, Z. *J. Phys. Chem. C* **2010**, *114*, 3874.
21. Peng, H.; Han, Y.; Liu, T.; Tjiu, W. C.; He, C. *Thermochim. Acta* **2010**, *502*, 1.
22. Then, Y. Y.; Ibrahim, N. A.; Yunus, W. M. Z. W. *J. Polym. Environ.* **2011**, *19*, 535.
23. Liao, C. Z.; Tjong, S. C. *Fatigue Fract. Eng. Mater. Struct.* **2011**, *35*, 56.
24. Fukushima, K.; Tabuani, D.; Abbate, C.; Arena, M.; Rizzarelli, P. *Eur. Polym. J.* **2011**, *47*, 139.
25. Muñoz-Bonilla, A.; Cerrada, M. L.; Fernández-García, M.; Kubacka, A.; Ferrer, M.; Fernández-García, M. *Int. J. Mol. Sci.* **2013**, *14*, 9249.
26. Saeed, K.; Park, S. Y. *J. Appl. Polym. Sci.* **2007**, *104*, 1957.
27. Abdolmohammadi, S.; Siyamak, S.; Ibrahim, N. A.; Yunus, W. M. Z. W.; Rahman, M. Z. A.; Azizi, S.; Fatehi, A. *Int. J. Mol. Sci.* **2012**, *13*, 4508.
28. Ramesh, N.; Carla, M.; Antonio, M.; Madhab, P. B.; Hak, Y. K.; Valerio, C. *Polymer* **2011**, *52*, 4054.
29. Hongdan, P. Y. H.; Tianxi, L.; Wuiwui, C. T.; Chaobin, H. *Thermochim. Acta* **2010**, *502*, 1.
30. Fukushima, K.; Abbate, C.; Tabuani, D.; Gennari, M.; Rizzarelli, P.; Camino, G. *Mater. Sci. Eng. C* **2010**, *30*, 566.